

Ultracold dense samples of dipolar RbCs molecules in the rovibrational and hyperfine ground state

Tetsu Takekoshi^{1,2}, Lukas Reichsöllner¹, Andreas Schindewolf¹, Jeremy M. Hutson³, C. Ruth Le Sueur³,
Olivier Dulieu⁴, Francesca Ferlaino¹, Rudolf Grimm^{1,2}, and Hanns-Christoph Nägerl¹

¹*Institut für Experimentalphysik, Universität Innsbruck, 6020 Innsbruck, Austria*

²*Institut für Quantenoptik und Quanteninformation,*

Österreichische Akademie der Wissenschaften, 6020 Innsbruck, Austria

³*Joint Quantum Centre (JQC) Durham/Newcastle, Department of Chemistry,
Durham University, South Road, Durham, DH1 3LE, United Kingdom*

⁴*Laboratoire Aimé Cotton, CNRS, Université Paris-Sud, Bat. 505, 91405 Orsay Cedex, France*

(Dated: March 1, 2022)

We produce ultracold dense trapped samples of $^{87}\text{Rb}^{133}\text{Cs}$ molecules in their rovibrational ground state, with full nuclear hyperfine state control, by stimulated Raman adiabatic passage (STIRAP) with efficiencies of 90%. We observe the onset of hyperfine-changing collisions when the magnetic field is ramped so that the molecules are no longer in the hyperfine ground state. A strong quadratic shift of the transition frequencies as a function of applied electric field shows the strongly dipolar character of the RbCs ground-state molecule. Our results open up the prospect of realizing stable bosonic dipolar quantum gases with ultracold molecules.

PACS numbers: 05.30.Rt, 33.20.-t, 42.62.Fi, 67.85.-d

DOI: 10.1103/PhysRevLett.113.205301

Samples of ultracold molecules with dipole moments that can be tuned with applied electric fields offer a platform for exploring many new areas of physics. They are good candidates to form many-body systems with features such as supersolidity, unconventional forms of superfluidity, and novel types of quantum magnetism [1–3]. They allow exquisite control over all quantum degrees of freedom, and offer the possibility of implementing quantum simulation protocols [4] that require genuine long-range interactions.

The most advanced experiments with ultracold polar molecules to date have been on KRb. Ni *et al.* [5] produced ultracold $^{40}\text{K}^{87}\text{Rb}$ molecules in states very close to dissociation by tuning a magnetic field across a Feshbach resonance, and transferred the resulting Feshbach molecules to the rovibrational absolute ground state by stimulated Raman adiabatic passage (STIRAP). Similar work has been carried out on non-dipolar Cs_2 [6, 7]. The ground-state KRb molecules can be transferred between hyperfine states using microwave radiation [8] and confined in one-dimensional [9] and three-dimensional [10] optical lattices. However, pairs of KRb molecules can undergo an exothermic chemical reaction to form $\text{K}_2 + \text{Rb}_2$; this provides an opportunity for studies of quantum state-controlled reactions [8, 9, 11], but also constitutes a loss mechanism for the trapped molecules.

There is great interest in producing samples of ultracold dipolar molecules that are collisionally stable. Żuchowski and Hutson [12] have shown that the molecules NaK, NaRb, NaCs, KCs and RbCs in their absolute ground states are stable to all possible 2-body collision processes. We have previously demonstrated that $^{87}\text{Rb}^{133}\text{Cs}$ Feshbach molecules can be produced from ultracold atoms by magneto-association [13, 14]. Similar

work has been reported by Köppinger *et al.* [15]. In this paper we describe the transfer of these molecules to their rovibrational ground state by STIRAP. We also demonstrate magnetic control and show that the resulting molecules decay much more slowly when they are in their hyperfine ground state than when they are in an excited hyperfine state.

The states and transitions involved in our ground-state molecule production process are shown in Fig. 1 (a)-(c). A pump laser beam L_p at 1557 nm couples a Feshbach state $|i\rangle$ with mostly $a^3\Sigma^+$ character to the $|v'=29\rangle$ level of the $b^3\Pi_1$ state with Rabi frequency Ω_p . This state has a small admixture of the $A^1\Sigma^+$ state [13, 16], and a dump laser beam L_d at 977 nm couples it to the rovibrational ground-state level $|v''=0, J''=0\rangle$ of the $X^1\Sigma^+$ potential with Rabi frequency Ω_d . This level is made up of 32 Zeeman sublevels, as shown in Fig. 1(c) [17]. At $B = 0$ the levels are grouped according to the total molecular nuclear spin $I'' = 2, 3, 4$, or 5. The stretched state with $M_{I''} = M_{\text{tot}} = 5$ is the absolute ground state for B larger than about 90 G. It can be accessed at $B = 181$ G using crossed vertical and horizontal linear polarizations (v_p, h_d) for L_p and L_d co-propagating in the horizontal plane.

We start by generating a sample of $^{87}\text{Rb}^{133}\text{Cs}$ Feshbach molecules via magneto-association in an ultracold, magnetically levitated and nearly quantum-degenerate mixture of Rb and Cs atoms. The molecules are initially produced using the Feshbach resonance at $B = 197.06$ G and then transferred by magnetic field ramps to the state $|-2(1,3)d(0,3)\rangle$ near $B = 180$ G as sketched in Fig. 1(b) and described in more detail in Ref. [14]. Here, states are labeled with quantum numbers $|n(f_{\text{Rb}}, f_{\text{Cs}})L(m_{f_{\text{Rb}}}, m_{f_{\text{Cs}}})\rangle$, where n is the vibrational

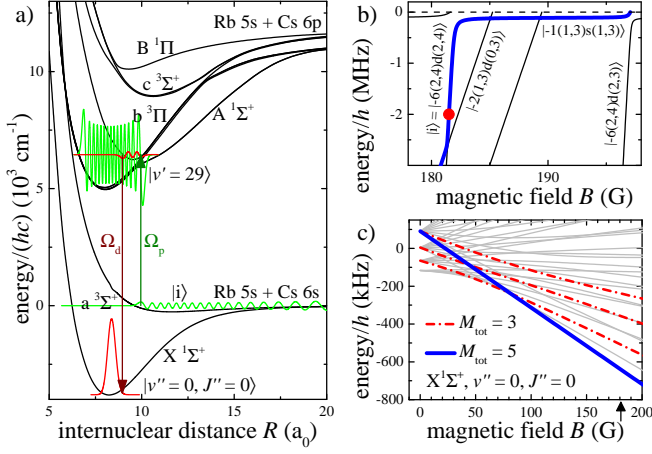


FIG. 1: (Color online). STIRAP scheme and levels involved. a) Ground- and excited-state molecular potentials of the RbCs molecule [13]. The transfer from the Feshbach state $|i\rangle$ at threshold to the rovibrational ground-state level $|v''=0, J''=0\rangle$ involves the $v'=29$ level belonging to the $b^3\Pi_1$ electronically excited state. The red and green solid lines indicate the wavefunctions that are coupled by the STIRAP pump and dump lasers L_p and L_d with Rabi frequencies Ω_p and Ω_d . b) Zeeman diagram for the states with $M_{\text{tot}} = 4$ just below the ground-state two-atom $(f_{\text{Rb}}, f_{\text{Cs}}) = (1, 3)$ threshold. The red dot marks the position from which STIRAP takes place. The magneto-association path is marked with a blue line. Energies are given relative to the field-dependent atomic dissociation threshold. c) Zeeman diagram showing the ground-state hyperfine structure (32 states). The magnetic field during STIRAP is indicated by the arrow. The energy levels are calculated using the Hamiltonian and parameters from Ref. [18]. The thick lines show the final states allowed by the selection rule $\Delta M_{\text{tot}} = \pm 1$ for vertical pump and horizontal dump polarization (v_p, h_d).

quantum number counted downwards from the $(f_{\text{Rb}}, f_{\text{Cs}})$ dissociation threshold, f indicates the atomic total angular momentum with projection m_f , and L is the molecular rotational angular momentum. We take the quantization axis to lie along the magnetic field direction, which is vertical in our setup [16].

The high-field-seeking molecules in state $|-2(1,3)d(0,3)\rangle$ are separated from the remaining atoms by the Stern-Gerlach effect. The magnetic field B is then ramped back up through the nearest avoided crossing to transfer the molecules into the strongly low-field-seeking state $|i\rangle = |-6(2,4)d(2,4)\rangle$ at a binding energy of approximately $2 \text{ MHz} \times h$ at $B = 181 \text{ G}$ (marked with a dot in Fig. 1(b)). This state is chosen because it has the greatest triplet fraction and the largest amplitude at short range, giving the most favorable Franck-Condon overlap for the STIRAP process described below. To reduce spatial Zeeman broadening and gravitational sag, the field gradient used for levitation is turned off and a vertical 1D optical lattice [16] is superimposed on the molecular cloud to

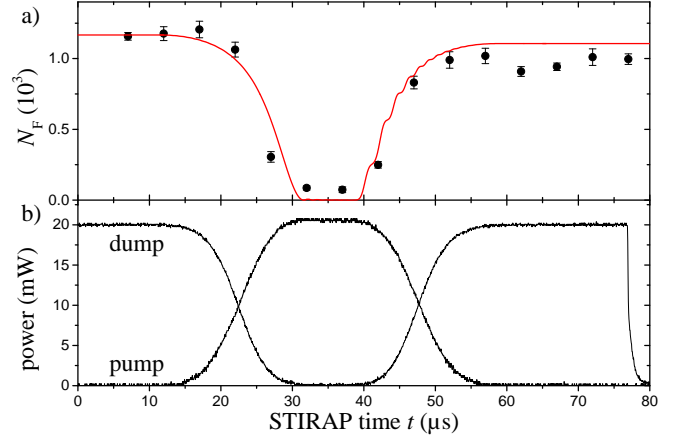


FIG. 2: (Color online). Efficient ground-state STIRAP transfer. a) Number of Feshbach molecules N_F as a function of STIRAP time t during a typical forward and reverse on-resonance STIRAP pulse sequence as shown in b). The peak Rabi frequencies are $\Omega_p = 2\pi \times 0.77(22) \text{ MHz}$ and $\Omega_d = 2\pi \times 2.3(6) \text{ MHz}$. The one-way STIRAP efficiency is 90%. The red curve is the result of a master equation model [16]. Error bars denote the 1σ standard statistical error. b) Laser power as a function of time t as recorded by photodiodes.

hold it against gravity. The molecular sample is thus held in a stack of pancake-shaped 2D traps with their tight axis along the vertical direction. This additional step, combined with the shorter collisional lifetime of molecules in the $n = -6$ state (about 30 ms), reduces the cloud population from 3000 to between 1000 and 1500 trapped molecules with a $1/e^2$ -cloud radius of between 30 and $40 \mu\text{m}$. The translational temperature measured in expansion after sudden release from the trap is $240(30) \text{ nK}$. The overall sample preparation procedure takes about 13 s.

STIRAP is based on a pulse sequence in which the dump laser is turned on before the pump laser to generate a transient dark superposition of the initial and final states [19]. We perform ground-state STIRAP from $|i\rangle$ to $|v''=0, J''=0\rangle$ and characterize its efficiency by reversing the STIRAP process as shown in Fig. 2 [20]. Molecules are transferred to the hyperfine-Zeeman ground state with $M_{\text{tot}} = 5$ between $t \approx 15$ and $30 \mu\text{s}$ and back to the Feshbach state $|i\rangle$ between $t \approx 40$ and $55 \mu\text{s}$. Both lasers are tuned to one-photon resonance for fixed $B = 181 \text{ G}$. The Feshbach molecules are then detected by dissociating them at the Feshbach resonance at 197.06 G and using absorption imaging on the atomic clouds [14]. The round-trip transfer efficiencies are typically about 80%, implying one-way transfer efficiencies of about 90%. For comparison, the solid line in Fig. 2(a) is the result of a simulation that takes laser linewidth into account, but not beam shape and laser noise pedestal effects [16]. It gives a somewhat higher efficiency.

Scanning the dump laser detuning Δ_d reveals hyperfine

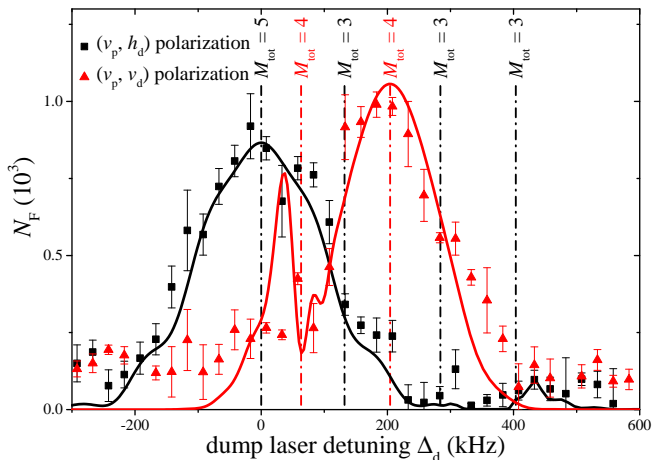


FIG. 3: (Color online). STIRAP spectrum showing the number of Feshbach molecules N_F after round-trip STIRAP as a function of dump laser detuning Δ_d for two different choices of the polarization of the dump laser. The energies of the hyperfine components of the ground state (calculated using the parameters of Ref. [18]) are marked with dashed vertical lines and labeled with their total angular momentum projection M_{tot} . For (v_p, h_d) polarization (black squares) the Feshbach molecules ($M_{\text{tot}} = 4$) are primarily transferred into the absolute hyperfine ground state with $M_{\text{tot}} = 5$. For (v_p, v_d) polarization (red triangles), hyperfine-excited levels are addressed. The solid curves are master equation simulation results [16]. The black curve centered around zero detuning is a fit to the data to determine the dump Rabi frequency. The Rabi frequencies are $\Omega_p = 2\pi \times 0.26(7)$ MHz and $\Omega_d = 2\pi \times 2.3(6)$ MHz.

and Zeeman substructure of the $X^1\Sigma^+$, $|v''=0, J''=0\rangle$ state as shown in Fig. 3. For (v_p, h_d) polarization the transfer is mostly into the level with $M_{\text{tot}} = 5$. For (v_p, v_d) polarization the transfer is primarily into one of the two hyperfine-excited levels with $M_{\text{tot}} = 4$. The most important terms in the ground-state hyperfine Hamiltonian [18] are the nuclear Zeeman shift and the scalar nuclear spin-spin interaction, which are governed by the electronic and nuclear g factors, and the nuclear spin-spin parameter c_4 , respectively. The second of these two terms dominates at low field. The g factors are very precisely known, and a simulation [16] using them and the c_4 parameter of Ref. [18] agrees well with the observed spectrum for both choices of polarisation.

There are usually 50 to 100 Feshbach molecules that remain after the transfer to the ground state (offset in Figs. 2(a) and 3). We believe this is mainly due to a slight beam misalignment and the fact that the molecular cloud and STIRAP beams have similar radii. We exclude these molecules when calculating the transfer efficiency. The efficiency is most likely limited by laser power, in the sense that Feshbach molecules at the edge of the cloud see lower laser intensities. Laser phase noise pedestals may also play a role, as discussed in Ref. [21].

To explore the molecules' collisional properties we

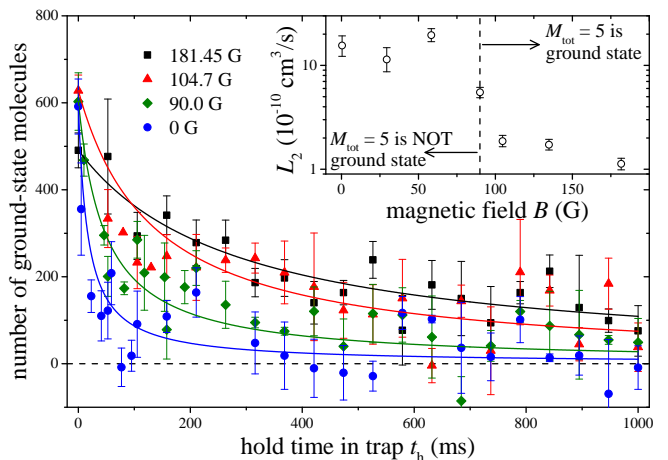


FIG. 4: (Color online). Decay of ground-state molecules as a result of collisions at zero electric field. The number of ground-state molecules in $M_{\text{tot}} = 5$ is plotted against hold time t_h in the crossed dipole trap for different values of the magnetic field B as indicated. The initial peak density is $1.1(1) \times 10^{11} \text{ cm}^{-3}$. The solid lines are fits based on a two-body decay model to determine the two-body loss rate coefficient L_2 [16]. The fits are constrained to run through the first data point at zero hold time. The inset plots L_2 as a function of B . A greatly reduced L_2 is seen at magnetic fields B greater than about 90 G, where the molecules are mostly in the hyperfine-Zeeman ground state.

load our sample of ground-state molecules into a three-dimensional crossed dipole trap [16]. The trap is comparatively stiff with a geometrically averaged trap frequency of 409(20) Hz to hold the sample against gravity. The sample's peak particle density is now $1.1(1) \times 10^{11} \text{ cm}^{-3}$. The compression of the sample leads to a marked increase in temperature to $8.7(7) \text{ } \mu\text{K}$. Nevertheless, we expect that s -wave collisions still dominate the collision process. Fig. 4 shows the ground-state population in the $M_{\text{tot}} = 5$ state as a function of hold time t_h between forward and reverse STIRAP transfer for various values of the magnetic field B . For this measurement, we first prepare the molecular sample as before at $B = 181 \text{ G}$ in $M_{\text{tot}} = 5$ and then ramp the magnetic field to the chosen value within about 1 ms. After time t_h we reverse the process and determine the remaining number of molecules. The results show ground-state molecule loss that depends strongly on B . Using a two-body decay model [16] we determine the two-body loss rate coefficient L_2 . Its dependence on B is shown in the inset to Fig. 4. The value of L_2 is considerably greater at fields below about 90 G. The state with $M_{\text{tot}} = 5$ is not the absolute ground state at fields below this threshold, as seen in Fig. 1(c), and we attribute the greatly reduced lifetime to hyperfine-changing collisions to form the lower-energy states. We note that L_2 is non-zero even for fields above 90 G; this may be due to thermal population of excited hyperfine states, or to losses involving long-lived collision

complexes [22, 23]. We also note that our ground-state sample is not 100% pure, because it initially contains some molecules left behind in the Feshbach state $|i\rangle$. The cross section for inelastic collisions between molecules in states $|M_{\text{tot}}=5\rangle$ and $|i\rangle$ is likely to be large, and will lead to some loss of ground-state molecules on the timescales considered here.

A crucial property of RbCs molecules is their permanent electric dipole moment μ , calculated to be 1.25 D in the absolute ground state [24, 25]. We have measured the Stark shift of the hyperfine ground state by applying voltages to a set of four parallel electrodes external to the fused silica cell vacuum chamber [16] and tracking the shift E_S of the $M_{\text{tot}}=5$ peak position (as in Fig. 3) from that recorded at zero electrode potential. The potential is pulsed to reduce charging effects from the alkali-coated cell walls [16, 26]. The resulting shift is shown in Fig. 5. Both the dump and the pump laser must be detuned considerably, because of the large excited-state shift shown in the inset of Fig. 5. The quadratic shift is observed to be $1.60(7)$ Hz/V², which implies a permanent dipole moment of $1.17(2)(4)$ D. Here, the first error is statistical, the second is the estimated systematic error due to geometrical uncertainty that enters when calculating the dielectrically enhanced electric field inside our quartz cell apparatus [16].

In conclusion, we have formed dense samples of ultracold RbCs molecules in their electronic and rovibrational ground state. The molecules are initially formed in near-dissociation states by magneto-association, and transferred to the ground state by the STIRAP method. The efficiency of the ground-state transfer is about 90%. With an appropriate choice of laser polarization, we can produce the molecules in their absolute hyperfine ground state. RbCs molecules in their ground state are stable to all possible two-body collision processes, so our results offer the prospect of producing the first collisionally stable quantum gas of dipolar molecules.

In future work, we will attempt to increase the sample size and density by creating Feshbach molecules from atomic Mott insulators in a three-dimensional optical lattice [27], in generalization of work on homonuclear Cs₂ [7]. The dynamics will then be dominated by nearest-neighbor interactions with interaction strength on the order of $\hbar \times 1$ kHz. This will allow us to study important problems in quantum many-body physics, such as the phase diagram of the Bose-Hubbard model extended by a long-range interaction term [28, 29].

We acknowledge contributions by V. Pramhaas, M. Kugler, and M. Debatin and thank N. Bouloufa, R. Vexiau, A. Crubellier and J. Aldegunde for fruitful discussions. We acknowledge support by the Austrian Science Fund (FWF) through the Spezialforschungsbereich (SFB) FoQuS within project P06 (FWF project number F4006-N23), the European Office of Aerospace Research and Development through Grant FA8655-10-1-3033 and

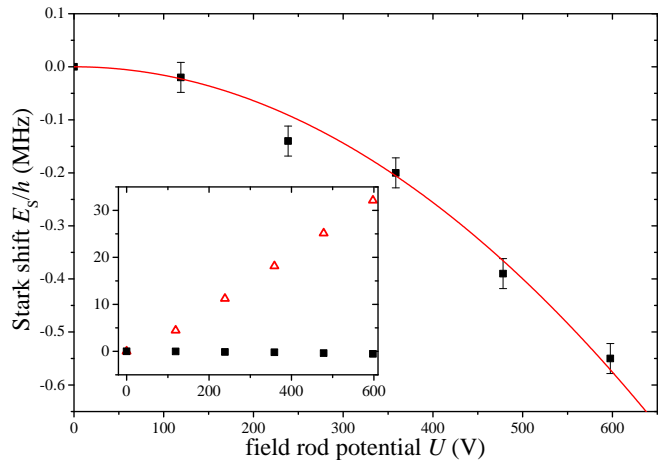


FIG. 5: (Color online). Stark shift of the $M_{\text{tot}}=5$ state of the RbCs ground state. The two-photon STIRAP resonance shift E_S is plotted as a function of the electrode potential U . The solid line is a quadratic fit. The inset shows an expanded range in which the excited-state shift can be seen as well (triangles).

the Engineering and Physical Sciences Research Council through Grant no. EP/I012044/1.

-
- [1] C. Trefzger, C. Menotti, B. Capogrosso-Sansone, and M. Lewenstein, *J. Phys. B: At. Mol. Opt. Phys.* **44**, 193001 (2011).
 - [2] M. Baranov, M. Dalmonte, G. Pupillo, and P. Zoller, *Chem. Rev.* **112**, 5012 (2012).
 - [3] T. Lahaye, C. Menotti, L. Santos, M. Lewenstein, and T. Pfau, *Rep. Prog. Phys.* **72**, 126401 (2009).
 - [4] I. Bloch, J. Dalibard, and S. Nascimbène, *Nature Phys.* **8**, 267 (2012).
 - [5] K.-K. Ni, S. Ospelkaus, M. H. G. de Miranda, A. Pe'er, B. Neyenhuis, J. J. Zirbel, S. Kotochigova, P. S. Julienne, D. S. Jin, and J. Ye, *Science* **322**, 231 (2008).
 - [6] J. G. Danzl, E. Haller, M. Gustavsson, M. J. Mark, R. Hart, N. Bouloufa, O. Dulieu, H. Ritsch, and H.-C. Nägerl, *Science* **321**, 1062 (2008).
 - [7] J. G. Danzl, M. J. Mark, E. Haller, M. Gustavsson, R. Hart, J. Aldegunde, J. M. Hutson, and H.-C. Nägerl, *Nature Phys.* **6**, 265 (2010).
 - [8] S. Ospelkaus, K.-K. Ni, G. Quémener, B. Neyenhuis, D. Wang, M. H. G. de Miranda, J. L. Bohn, J. Ye, and D. S. Jin, *Phys. Rev. Lett.* **104**, 030402 (2010).
 - [9] M. H. G. de Miranda, A. Chotia, B. Neyenhuis, D. Wang, G. Quémener, S. Ospelkaus, J. L. Bohn, J. Ye, and D. S. Jin, *Nature Phys.* **7**, 502 (2011).
 - [10] A. Chotia, B. Neyenhuis, S. A. Moses, B. Yan, J. P. Covey, M. Foss-Feig, A. M. Rey, D. S. Jin, and J. Ye, *Phys. Rev. Lett.* **108**, 080405 (2012).
 - [11] K.-K. Ni, S. Ospelkaus, D. Wang, G. Quemener, B. Neyenhuis, M. H. G. de Miranda, J. L. Bohn, J. Ye, and D. S. Jin, *Nature* **464**, 1324 (2010).
 - [12] P. S. Żuchowski and J. M. Hutson, *Phys. Rev. A* **81**,

- 060703(R) (2010).
- [13] M. Debatin, T. Takekoshi, R. Rameshan, L. Reichsöllner, F. Ferlaino, R. Grimm, R. Vexiau, N. Bouloufa, O. Dulieu, and H.-C. Nägerl, *Phys. Chem. Chem. Phys.* **13**, 18926 (2011).
 - [14] T. Takekoshi, M. Debatin, R. Rameshan, F. Ferlaino, R. Grimm, H.-C. Nägerl, C. R. Le Sueur, J. M. Hutson, P. S. Julienne, S. Kotochigova, et al., *Phys. Rev. A* **85**, 032506 (2012).
 - [15] M. P. Köppinger, D. J. McCarron, D. L. Jenkin, P. K. Molony, H.-W. Cho, S. L. Cornish, C. R. Le Sueur, C. L. Blackley, and J. M. Hutson, *Phys. Rev. A* **89**, 033604 (2014).
 - [16] See Supplemental Material for details on the molecular states, on laser light generation, on the optical lattice, on modeling the STIRAP time course, on the two-body decay model, and on the DC-Stark shift measurement setup.
 - [17] J. Aldegunde and J. M. Hutson, *Phys. Rev. A* **79**, 013401 (2009).
 - [18] J. Aldegunde, B. A. Rivington, P. S. Żuchowski, and J. M. Hutson, *Phys. Rev. A* **78**, 033434 (2008).
 - [19] K. Bergmann, H. Theuer, and B. W. Shore, *Rev. Mod. Phys.* **70**, 1003 (1998).
 - [20] M. Debatin, Ph.D. thesis, University of Innsbruck (2013).
 - [21] L. P. Yatsenko, B. W. Shore, and K. Bergmann, *Phys. Rev. A* **89**, 013831 (2014).
 - [22] M. Mayle, G. Quémener, B. P. Ruzic, and J. L. Bohn, *Phys. Rev. A* **87**, 012709 (2013).
 - [23] K. Lauber, E. Kilirov, M. J. Mark, F. Meinert, and H.-C. Nägerl, to be published.
 - [24] M. Aymar and O. Dulieu, *J. Chem. Phys.* **122**, 204302 (2005).
 - [25] S. Kotochigova and E. Tiesinga, *J. Chem. Phys.* **123**, 174304 (2005).
 - [26] M. A. Bouchiat, J. Guena, P. Jacquier, M. Lintz, and A. V. Papoyan, *Appl. Phys. B* **68**, 1109 (1999).
 - [27] A. Lercher, T. Takekoshi, M. Debatin, B. Schuster, R. Rameshan, F. Ferlaino, R. Grimm, and H.-C. Nägerl, *Eur. Phys. J. D* **65**, 3 (2011).
 - [28] B. Damski, L. Santos, E. Tiemann, M. Lewenstein, S. Kotochigova, P. Julienne, and P. Zoller, *Phys. Rev. Lett.* **90**, 110401 (2003).
 - [29] B. Capogrosso-Sansone, C. Trefzger, M. Lewenstein, P. Zoller, and G. Pupillo, *Phys. Rev. Lett.* **104**, 125301 (2010).

SUPPLEMENTAL MATERIAL

Molecular states involved

In contrast to the case of homonuclear alkali dimers, whose excited states have a resonant dipole-dipole van der Waals interaction, in heteronuclear dimers the excited and ground states both have $1/R^6$ van der Waals interactions, where R is the internuclear distance. This makes it more likely that a suitable excited state exists that simultaneously has good Franck-Condon overlap with the Feshbach and ground states, making four-photon transfer schemes unnecessary [1].

We initially chose laser wavelengths to address states of the strongly coupled $A^1\Sigma^+ - b^3\Pi_{0+}$ system but found the ground-state transfer efficiency to be extremely poor, even though the predicted and measured laser couplings were strong. A transition to the $b^3\Pi_1$, $|v'=29\rangle$ state [2] worked much better and the results using this intermediate state are presented in this work. We attribute the low $A^1\Sigma^+ - b^3\Pi_{0+}$ transfer efficiency to the fact that Zeeman and hyperfine splittings in $\Omega'=0$ states are much smaller than our one-photon STIRAP linewidth ($\sim \Omega_{p0}\Omega_{d0}\tau_p$, where Ω_{p0} and Ω_{d0} are the peak pump and dump Rabi frequencies and τ_p is the STIRAP-pulse overlap time [3]). In this case, multiple intermediate states are addressed simultaneously, which causes loss [4–6]. While this can often be remedied by detuning far from all intermediate states, large Rabi frequencies are often required. In STIRAP of Cs₂ [1], where the magnetic field is low enough that the total angular momentum F is nearly a good quantum number, a fixed ratio between the dump and pump Rabi frequencies of the multiple intermediate states exists and the losses are ameliorated [6].

Decomposing the Feshbach state $|i\rangle$ into its Hund's case (a) nuclear-spin decoupled basis states reveals it to be a superposition of $J=1, 2$ and 3 with only the $J=1$ component coupling to $b^3\Pi_1, J'=1$ due to the selection rules $\Delta J=0, \pm 1$ and $\Delta \Sigma=0$. Here J is the total molecular angular momentum excluding nuclear spin and Σ is the projection of the total electron spin onto the internuclear axis. The intermediate $b^3\Pi_1$ state is actually not expected to allow coupling to the $X^1\Sigma^+$ ground state due to the selection rule $\Delta S=0$. However, the $v'=29, J'=1$ level of $b^3\Pi_1$ system lies only 16 GHz away [2] from the $v'=38, J'=1$ level of the $A^1\Sigma^+ - b^3\Pi_{0+}$ system and contains a small admixture of $A^1\Sigma^+, J'=1$ [7], which can be coupled to the $X^1\Sigma^+, J''=0$ ground state. The calculated vibrational wavefunctions for both intermediate components are indicated in Fig. 1 of the main text. A small admixture of $B^1\Pi$ is also possible and cannot be ruled out [8]. The $b^3\Pi_1, J'=1$ hyperfine and Zeeman manifold spans about $h \times 700$ MHz and we empirically found the state with the strongest couplings using π (vertically) polarized pump light and $\sigma^+ - \sigma^-$

(horizontally) polarized dump light.

At $B=181$ G the absolute ground state is the stretched $M_{\text{tot}}=5$ state. This has the same nuclear spin orientation $m_{i_{\text{Rb}}}=3/2, m_{i_{\text{Cs}}}=7/2$ as the initial Feshbach state, implying that the intermediate state must also have high $m_{i_{\text{Rb}}}=3/2, m_{i_{\text{Cs}}}=7/2$ character for good transfer efficiency. This is indeed the case. Subsequent spectroscopy and analysis of the $b^3\Pi_1, v'=29, J'=1$ state [9] has revealed that the lowest of the 18 allowed transitions of the intermediate state manifold gives the strongest one-photon coupling and has quantum numbers $M_{\text{tot}}=4, J'=1, m_{J'} \approx -1, m_{i_{\text{Rb}}} \approx 3/2$, and $m_{i_{\text{Cs}}} \approx 7/2$. Our intermediate state model gives us a complete picture of the possibilities for direct transfer to other $X^1\Sigma^+, J''=0$ states should the need arise.

Laser light generation

The pump and dump STIRAP light is derived from diode lasers that are stabilized via phase locks using additional transfer diode lasers and tunable radiofrequency sources to two independent high-finesse cavities [10] with finesse $F=240,000$ and $440,000$, respectively. Each laser can be tuned by hundreds of MHz with radiofrequency precision and delivers a little over 20 mW into a beam with a $1/e^2$ intensity radius of about $40 \mu\text{m}$ at the position of the molecular sample. The short-term laser linewidths inferred from the lock signals are approximately 90 and 170 Hz and the measured broadening due to acoustic effects in the optical fibers used for beam delivery is less than 70 Hz.

Optical lattice

The 1D optical lattice is generated by narrow-band laser light at $\lambda=1064.5$ nm propagating along the vertical z -direction. The light with a power up to $P=0.8$ W is collimated to a beam with $1/e^2$ -radius of $415 \mu\text{m}$ at the position of the molecular sample. The depth of the lattice is about $V_z = 48E_{\text{R}}^{\text{RbCs}}$ at $P=0.34$ W, where $E_{\text{R}}^{\text{RbCs}} = \hbar^2/(2m_{\text{RbCs}}\lambda^2) = \hbar \times 0.8$ kHz is the photon recoil energy, with m_{RbCs} the mass of the RbCs molecule. At such a depth, tunneling from well to well is fully suppressed.

Modeling the STIRAP time course

To simulate the STIRAP process we use a master equation in Lindblad form [11]. The effects of finite laser linewidths are included in the model, but the effects of beam shape and phase noise pedestals are not. The basis set contains the Feshbach state, the excited state, and the

lowest 10 hyperfine and Zeeman ground states. All parameters except the Franck-Condon factor for the dump transition are either known or have been measured. This factor is varied until the black theory curve fits the data near the main (v_p , h_d) peak shown in Fig. 3 of the main text.

From the natural linewidth of the excited level $|v' = 29\rangle$, measured to be 135(10) kHz, along with a one-photon on-resonance absorption measurement [12], we obtain a pump Rabi frequency of $\Omega_p = 2\pi \times 0.84(24)\text{kHz} \sqrt{I_p/(\text{mW}/\text{cm}^2)}$, where I_p is the pump laser intensity. We estimate the dump Rabi frequency by varying it until the ground-state transfer simulation roughly agrees with the (v_p , h_d) polarization data (Fig. 3). This gives a dump Rabi frequency of $\Omega_d = 2\pi \times 2.76(67)\text{kHz} \sqrt{I_d/(\text{mW}/\text{cm}^2)}$, where I_d is the pump laser intensity.

Crossed dipole trap and two-body decay model

We perform the collisional measurements in a crossed dipole trap whose trap frequencies are $(\omega_x, \omega_y, \omega_z) = 2\pi \times (439, 294, 529)$ Hz in the horizontal (x, y) and vertical (z) directions. For modeling the decay we assume a Gaussian spatial distribution for a sample that remains in (quasi) thermal equilibrium at temperature T . The rate equation for the density of ground-state molecules n_g reads

$$\dot{n}_g = -L_2 n_g^2$$

with the two-body loss rate coefficient L_2 . Here, we assume that the decay is dominated by a two-body process. Introducing the effective volume $V_{\text{eff}} = (m\bar{\omega}^2/(4\pi k_B T))^{-3/2}$, where $\bar{\omega}$ is the geometrically averaged trap frequency $\bar{\omega} = (\omega_x \omega_y \omega_z)^{1/2}$, allows us to rewrite this equation in the form

$$\dot{N}_g = -(L_2/V_{\text{eff}})N_g^2,$$

where N_g is the number of ground-state molecules. We fit solutions to this equation to the data shown in Fig. 4 to determine L_2 as shown in the inset to Fig. 4. We note that an attempt to model our data assuming just a one-body loss process fails a chi-squared test.

DC-Stark shift measurement setup

We apply an electric field by putting voltages on four nearly parallel 8.0 mm-diameter 140 mm-long external rod electrodes at the corners of the rectangular-cross-sectioned fused silica vacuum cell. The rods are separated by 52.0(1) mm along the vertical direction and by 68(1) mm horizontally. The position of the molecular sample with respect to the electrodes is known to about 1 mm. We estimate the field from this geometry to be 60(3)% of the value expected from infinitely wide parallel plates separated by 52.0 mm.

-
- [1] J. G. Danzl, M. J. Mark, E. Haller, M. Gustavsson, R. Hart, J. Aldegunde, J. M. Hutson, and H.-C. Nägerl, *Nature Phys.* **6**, 265 (2010).
 - [2] M. Debatin, T. Takekoshi, R. Rameshan, L. Reichsöllner, F. Ferlaino, R. Grimm, R. Vexiau, N. Bouloufa, O. Dulieu, and H.-C. Nägerl, *Phys. Chem. Chem. Phys.* **13**, 18926 (2011).
 - [3] N. V. Vitanov and S. Stenholm, *Opt. Comm.* **135**, 394 (1997).
 - [4] B. W. Shore, J. Martin, M. P. Fewell, and K. Bergmann, *Phys. Rev. A* **52**, 566 (1995).
 - [5] J. Martin, B. W. Shore, and K. Bergmann, *Phys. Rev. A* **52**, 583 (1995).
 - [6] N. V. Vitanov and S. Stenholm, *Phys. Rev. A* **60**, 3820 (1999).
 - [7] O. Docenko, M. Tamanis, R. Ferber, T. Bergeman, S. Kotochigova, A. V. Stolyarov, A. de Faria Nogueira, and C. E. Fellows, *Phys. Rev. A* **81**, 042511 (2010).
 - [8] S. Kotochigova, private communication.
 - [9] T. Takekoshi, R. Grimm, and H.-C. Nägerl, to be published.
 - [10] J. Alnis, A. Matveev, N. Kolachevsky, T. Udem, and T. W. Hänsch, *Phys. Rev. A* **77**, 053809 (2008).
 - [11] C. W. Gardiner and P. Zoller, *Quantum Noise* (Springer, Berlin-Heidelberg, 2010).
 - [12] T. Takekoshi, M. Debatin, R. Rameshan, F. Ferlaino, R. Grimm, H.-C. Nägerl, C. R. Le Sueur, J. M. Hutson, P. S. Julienne, S. Kotochigova, et al., *Phys. Rev. A* **85**, 032506 (2012).